Earth and Planetary Science Letters 489 (2018) 123–134

Contents lists available at ScienceDirect

Earth and Planetary Science Letters

www.elsevier.com/locate/epsl

Infiltration-driven metamorphism, New England, USA: Regional CO_2 fluxes and implications for Devonian climate and extinctions

E.M. Stewart *, Jay J. Ague

Yale University Department of Geology & Geophysics, P.O. Box 208109, New Haven, CT 06520-8109, United States

ARTICLE INFO

Article history:
Received 7 November 2017
Received in revised form 7 February 2018
Accepted 22 February 2018
Available online 8 March 2018
Editor: M. Bickle

Keywords:
metamorphic decarbonation
thermodynamic modeling
fluid infiltration
metamorphic carbon flux

ABSTRACT

We undertake thermodynamic pseudosection modeling of metacarbonate rocks in the Wepawaug Schist, Connecticut, USA, and examine the implications for CO_2 outgassing from collisional orogenic belts. Two broad types of pseudosections are calculated: (1) a fully closed-system model with no fluid infiltration and (2) a fluid-buffered model including an H_2O–CO_2 fluid of a fixed composition. This fluid-buffered model is used to approximate a system open to infiltration by a water-bearing fluid. In all cases the fully closed-system model fails to reproduce the observed major mineral zones, mineral compositions, reaction temperatures, and fluid compositions. The fluid-infiltrated models, on the other hand, successfully reproduce these observations when the X_{CO_2} of the fluid is in the range ~0.05 to ~0.15. Fluid-infiltrated models predict significant progressive CO_2 loss, peaking at ~50% decarbonation at amphibolite facies. The closed-system models dramatically underestimate the degree of decarbonation, predicting only ~15% CO_2 loss at peak conditions, and, remarkably, <1% CO_2 loss below ~600 °C. We propagate the results of fluid-infiltrated pseudosections to determine an areal CO_2 flux for the Wepawaug Schist. This yields $\sim 10^{12}$ mol CO_2 km^{-2} Myr^{-1}, consistent with multiple independent estimates of the metamorphic CO_2 flux, and comparable in magnitude to fluxes from mid-ocean ridges and volcanic arcs. Extrapolating to the area of the Acadian orogenic belt, we suggest that metamorphic CO_2 degassing is a plausible driver of global warming, sea level rise, and, perhaps, extinction in the mid- to late-Devonian.

1. Introduction

Since the turn of the twentieth century, the scientific community has recognized the global carbon cycle's effect on Earth's climate (Arrhenius and Sandström, 1903; Chamberlain, 1899). Geochemical box models (e.g. Berner, 1989) are commonly used to understand the mass balance associated with carbon cycling. While these models continue to improve, our progress in understanding the history of the global carbon cycle is ultimately limited by our knowledge of carbon fluxes in the past. In particular, the addition of CO_2 to the atmosphere via metamorphic processes remains poorly constrained. With estimates for the metamorphic carbon flux varying by well over an order of magnitude (e.g. Dasgupta and Hirschmann, 2010; Hayes and Waldbauer, 2006; Keleman and Manning, 2015; Kump et al., 2000), it is clear that more observational constraints are needed.

Decarbonation can be significantly enhanced by the infiltration of a water-bearing fluid during prograde metamorphism (e.g. Ferry, 1976, 1992, 1994, 2016; Ferry et al., 2013; Kerrick, 1977). Infiltration of H_2O lowers the activity of CO_2 in the fluid which drives reaction progress and increases CO_2 production as the system attempts to return to equilibrium (e.g. Kerrick, 1977). These CO_2-producing reactions are strongly dependent on fluid composition and cannot be modeled without knowledge of the amount and nature of fluid infiltration. Most significantly, a closed-system model may underestimate the degree of decarbonation and the mass of metamorphic CO_2 which is released. This effect is most pronounced at moderate temperatures (e.g. greenschist, amphibolite facies), when the infiltrating fluid has a relatively low concentration of CO_2, or when the time-integrated fluid flux is high.

Despite these complications, the fully closed-system approach to modeling metamorphism is common. With the relatively recent advent of pseudosection modeling (Connolly and Petrini, 2002; De Capitani and Petrakakis, 2010; Powell et al., 1998) it has become computationally efficient to calculate pressure–temperature phase diagrams for a fixed bulk composition. This tool is often utilized to estimate the pressure–temperature conditions reached by a rock with the assumption that the bulk composition observed today represents the rock's composition during the metamorphic stage of interest.

In particular, the classic closed-system decarbonation calculations of Kerrick and Connolly (2001a, 2001b) were instrumental in

* Corresponding author.
E-mail address: emily.stewart@yale.edu (E.M. Stewart).

https://doi.org/10.1016/j.epsl.2018.02.028
0012-821X/

forming a basis for models hypothesizing that subducted lithologies undergo minimal CO_2 loss during prograde reaction. Similar modeling has been applied in collisional settings (e.g. Groppo et al., 2013, 2017). Gorman et al. (2006) demonstrate that limited fluid infiltration during subduction will drive decarbonation reactions, but suggest that the majority of carbon still remains as a solid in the subducting slab. Importantly, these results are sensitive to the degree of fluid infiltration; a more heavily infiltrated slab would be expected to release more CO_2 via metamorphism (Gorman et al., 2006).

Many global models do not explicitly account for continental decarbonation (e.g. Jagoutz et al., 2016), and some papers suggest it is negligible except at very high temperatures (e.g. Dasgupta, 2013). High temperature reaction is certainly a viable means to release CO_2, but fluid infiltration can depress the temperatures of decarbonation reactions and allow for significant carbon loss even at moderate metamorphic grades. Thus, constraining the nature and magnitude of fluid infiltration is essential to further consideration of metamorphic devolatilization and its impact on global-scale carbon cycling.

We therefore aim to constrain the extent to which open-system processes (e.g. fluid infiltration) were at play in a Barrovian metamorphic setting. By testing the viability of both open- and closed-system models, we can constrain the degree and nature of fluid infiltration during metamorphism and its effect on decarbonation. Ideally we would acquire this constraint using an efficient and computationally simple approach.

With these considerations in mind, we present the results of systematic thermodynamic modeling of regionally metamorphosed carbonate rocks from the Wepawaug Schist, Connecticut. This serves as a proof-of-concept for the use of closed-system thermodynamic modeling to constrain the history of metamorphic fluid infiltration. We calculate two broad types of pseudosections using bulk compositions measured in low-grade precursor rocks: (1) a fully closed-system model with no fluid infiltration and (2) fluid-buffered models including an H_2O–CO_2 fluid of a fixed composition. Consequently, we utilize closed-system modeling to consider the open-system process of fluid infiltration and its effect on metamorphic decarbonation.

Finally, we extrapolate these results to estimate a CO_2 flux for the metamorphism of the Wepawaug Schist and the Acadian orogenic belt as a whole. We compare this result to independent metamorphic flux estimates from the literature, and consider the timing of CO_2 release and its relationship to Devonian climate, sea level, and extinction events.

2. Geological setting

The Wepawaug Schist in southern Connecticut consists primarily of metapelitic rocks with intercalated metapsammitic beds and impure metacarbonate rocks which underwent Barrovian-style metamorphism during the Acadian orogeny from ~410 to ~380 Ma (Lancaster et al., 2008; Lanzirotti and Hanson, 1996). It is lithologically similar to the Waits River Formation in eastern Vermont which was the subject of multiple classic studies on metamorphic decarbonation in New England (e.g. Ferry, 1992; Léger and Ferry, 1993). The metaclastic rocks account for ~90% of the unit volume; metacarbonate beds are on the order of 1 cm up to 10 m thick with most falling in the range of ~10 to ~100 cm. Metamorphic grade increases from east to west with metapelitic rocks ranging from chlorite-zone conditions up to the staurolite–kyanite zone. The pressure was ~7 to 9 kbars and peak temperatures range from ~420 °C to ~625 °C (Ague, 1994, 2002; Hewitt, 1973).

Metacarbonate rocks can be broadly separated into four metamorphic zones. From lowest to highest grade they are the ankerite, biotite, amphibole, and diopside zones (Ague, 1994, 2002; Fritts, 1963, 1965a, 1965b; Hewitt, 1973; Palin, 1992), similar to elsewhere in New England (e.g. Ferry, 1992) (Fig. 1). Importantly, thermobarometry in the metapelitic beds allows us to constrain the spatial variation in P–T conditions (e.g. Ague, 1994, 2002; Hewitt, 1973) and then apply these robust constraints to the intercalated metacarbonate rocks. Additionally, the mole fraction of CO_2 in the metamorphic fluid (X_{CO_2}) has been previously constrained to lie between 0.01 and 0.15 for most samples – Ague (2002) estimates X_{CO_2} using the program TWQ (Berman, 1991) together with measured mineral compositions and field-based P–T estimates. Tracy et al. (1983) find consistent results using mineral equilibria from the three independent decarbonation reactions they observed. Thus, this unit offers an ideal opportunity to test the viability of open- versus closed-system modeling for the decarbonation of metamorphic rocks in a well-understood regional metamorphic setting at a large scale and over a range of metamorphic grades.

3. Sample description

Eight samples from the lowest grade ankerite zone were considered in this study (sample names in Appendix A; see Ague, 2002, 2003 for detailed sample descriptions). They have not undergone large amounts of metamorphic CO_2 loss but are otherwise similar in composition to the higher-grade rocks of the biotite, amphibole, and diopside zones (Ague, 2003). We therefore use their modern bulk compositions to represent the precursors of the higher-grade rocks. By forward modeling the metamorphism of these low-grade rocks up to higher temperatures we expect to reproduce the observed mineral zones and volatile changes.

Herein we focus our analysis on three representative samples – 184a, 189a, and Wep-29a. They contain calcite + ankerite + muscovite + quartz + rutile + plagioclase; samples 184a and 189a contain albite whereas sample Wep-29a has a higher Na/K ratio and instead contains abundant oligoclase. It is likely that at lower-grade Wep-29a contained paragonite, but it was consumed to produce plagioclase (Ague, 2003). Samples also contain minor graphite/organic carbon that likely contributed a small amount of methane to the metamorphic fluid. However, the mole fraction of methane in the fluid (X_{CH_4}) should be small ($<$~0.02) at the relevant P–T conditions (e.g. Ague, 2002; Chu and Ague, 2013), and we therefore ignore this component. In addition, there is minor pyrite (and at higher grades pyrrhotite) in some samples. However, at $<$1 wt% the bulk sulfur content of the samples is small and will have little effect on phase assemblages (Evans et al., 2010).

In addition, we consider sample W5, a higher-grade rock from the amphibole zone. W5 is of interest because its phase equilibria record an anomalously high X_{CO_2} for the region (Ague, 2002). Thus, W5 may record some different conditions or processes. It contains calcite + quartz + plagioclase + biotite + clinozoisite + amphibole + garnet + titanite. Despite reaching temperatures in excess of 600 °C, there is no evidence that W5 ever contained diopside (Hewitt, 1973; Ague, 2002).

The molar composition of each sample used for pseudosection modeling is given in Appendix A (Table A1), together with calculation details.

4. Methods

We perform two types of pseudosection modeling in the system NCKFMASHTC using Theriak-Domino (De Capitani and Petrakakis, 2010) and the thermodynamic data of Holland and Powell (1998) together with compatible activity models (Appendix A). The first type of pseudosection assumes the rocks were reacting in a fully closed-system that is well represented by the modern measured

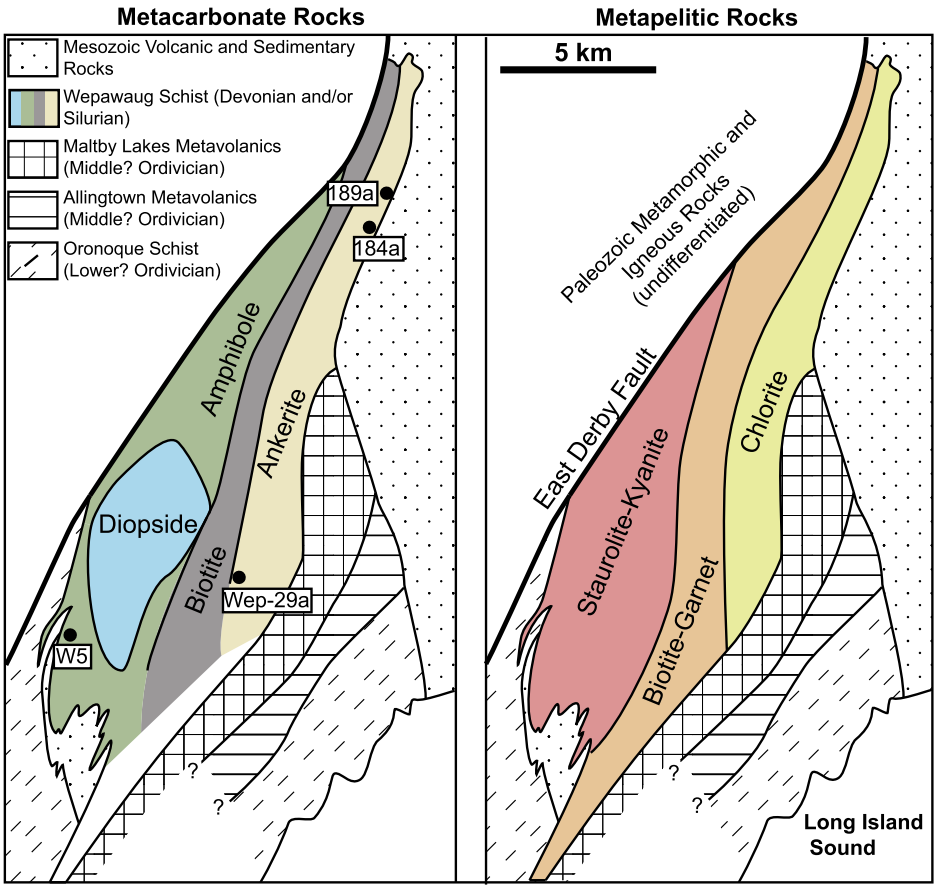

Fig. 1. Geologic map of the Wepawaug Schist, modified after Ague (2003). Black dots indicate sampling locations. (For interpretation of the colors in the figure(s), the reader is referred to the web version of this article.)

bulk composition of the rocks. For the fully closed-system models of low-grade precursors the modern measured CO_2 and H_2O contents are used (see Ague, 2003 for the conversion of loss-on-ignition (LOI) to wt% CO_2 and H_2O). Sample W5 is higher grade and lost significant CO_2 and H_2O during metamorphism; thus, we corrected its measured composition for volatile loss (Appendix A).

In addition to pseudosection modeling, we calculate the fluid compositions predicted by these closed-system models for all samples. Two different approaches are used; the first assumes a fully closed system where no fluid enters or escapes (e.g. Kerrick and Connolly, 2001a, 2001b). We also calculate fluid compositions assuming Rayleigh-type distillation (e.g. Greenwood, 1975) where each parcel of fluid created from metamorphic devolatilization is removed at a given temperature increment using a step size of 5 °C. For all of the calculations the temperature is increased from 400 to 650 °C and pressure is fixed at a representative value of 8 kbars.

The second category of modeling utilizes closed-system pseudosections to explore the open-system process of fluid infiltration. We begin with the same modern molar composition as described above, but we add a very large amount of C and H to the reacting system. The molar ratio of C to H – and therefore X_{CO_2} of the fluid – is fixed at some predetermined value. This effectively allows us to place the reactive solid in contact with a buffering fluid of fixed composition; no amount of reaction with the smaller rock reservoir can significantly change the composition of the fluid, whereas the fluid can exert control on the phase equilibria in the solid. We refer to these models broadly as "fluid-infiltrated" herein.

In nature, the fluid composition was not fixed; reaction with the solid rock would shift the composition of the fluid somewhat during reaction (Ague and Rye, 1999). As a water-rich fluid enters the system, it lowers X_{CO_2} to values that are not in equilibrium with the mineral assemblage; this drives decarbonation reactions (e.g. Kerrick, 1977; Ferry, 1992). The release of CO_2 via decarbonation increases the fluid X_{CO_2}, resulting in a fluid composition that approaches equilibrium. In a system with continuous infiltration, a given reaction will closely (but not exactly) follow the equilibrium curve on a T–X_{CO_2} diagram. A major difference, however, between this behavior and closed- or Rayleigh-type behavior is that the reaction progress is greater in the infiltration case. (Of course, large reaction progress is also possible at or near isobaric consolute or invariant points.) When a reactant is exhausted, CO_2 production stops but infiltration continues, lowering X_{CO_2} until a fluid composition appropriate for the next reaction is reached. CO_2 is once again evolved, and the process repeats. This ultimately produces a "zig-zag" pattern on T–X_{CO_2} diagrams defined by the reaction sequence (e.g. Fig. 3 in Ague and Rye, 1999).

Fig. 2 depicts hypothetical fluid evolution paths on a T–X_{CO_2} diagram. The path for a moderate volume of fluid infiltration is shown in pink, highlighting the "zig-zag" behavior described above. By fixing the X_{CO_2} (green path), we create a model which closely – though imperfectly – approximates the pink path. The change in the X_{CO_2} of this moderate-volume fluid is relatively small, especially in comparison to the large range of CO_2 concentrations predicted by closed-system and Rayleigh-like models. Thus, the fluid-buffered model is a good approximation of real-world (moderate volume) infiltration. Importantly, this result can be calculated with a simple pseudosection, as opposed to the solution of coupled partial differential equations describing advection, dispersion, and reaction as in Ague and Rye (1999).

For each of the samples, fourteen phase diagrams were calculated: closed-system pseudosections, and fluid-infiltrated pseu-

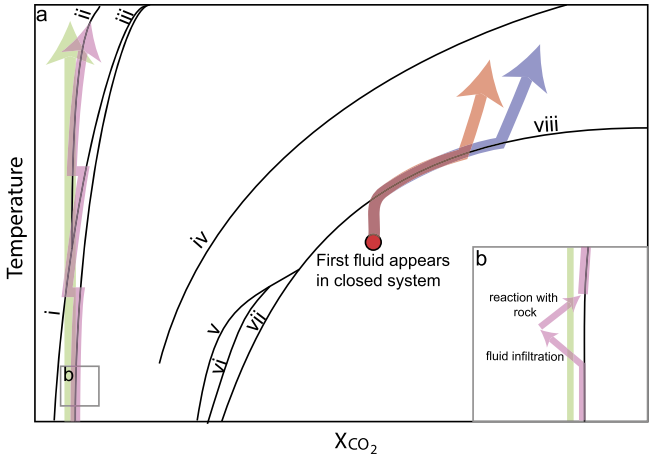

Fig. 2. a) Schematic isobaric T–X_{CO_2} diagram; Black curves are univariant reaction curves. Red and blue lines represent fully-closed and Rayleigh-like systems respectively. The pink line represents a realistic path for fluid infiltration (e.g. Ague and Rye, 1999). The green line is the fixed X_{CO_2} simplification made in our models. b) A zoomed-in view of fluid evolution along a reaction curve in which infiltration by a low X_{CO_2} fluid drives the X_{CO_2} to lower values and decarbonation of the solid rock drives the X_{CO_2} back towards a higher value.

dosections at $X_{CO_2} = 0.025, 0.05, 0.075, 0.10, 0.15$, and 0.20 using both the Franzolin et al. (2011) carbonate activity model and a simple carbonate activity model (Holland and Powell, 1998). As the simple carbonate model gave qualitatively similar results to the Franzolin et al. (2011) model, we present only the Franzolin et al. (2011) results.

We calculate the amount of carbon remaining in the solid rock for each low-grade sample using three models: a fully closed-system, a semi-open-system with Rayleigh-like distillation, and fluid-infiltrated models at $X_{CO_2} = 0.05, 0.75$, and 0.10. As above, temperature is increased from 400 to 650 °C in increments of 5 °C and pressure is fixed at 8 kbars.

5. Results

5.1. P–T pseudosections

Fig. 3 shows P–T pseudosections for samples 184a, 189a, and Wep-29a. (Without exception, the results from the remaining five low-grade samples are consistent with results in Fig. 3 and therefore they are not discussed in detail.) Gray shaded regions indicate a phase field containing calcite and ankerite whereas red phase fields include only calcite. For each of these samples the closed-system pseudosection qualitatively fails to reproduce the progression of major mineral zones observed in the field. In contrast, each of the models calculated with a fluid composition of $X_{CO_2} = 0.05$ generally matches our field observations well; they all contain a biotite-in reaction approximately coincident with the ankerite-out reaction, and at higher grades they predict a Ca-amphibole zone followed by a diopside zone at peak temperatures.

5.2. Reaction temperatures

The ankerite-out reaction occurred between ~500 and ~530 °C based on calcite–ankerite thermometry and its correspondence to the biotite-in reaction in the intercalated metapelitic rocks (Hewitt, 1973; Ague, 2002). Biotite-, amphibole-, and diopside-in reactions occurred at ~510, ~530, and ~575 °C, respectively (Ague, 2002). We can therefore compare the results of each type of model to these independently-constrained reaction temperatures for a more quantitative assessment of their viability.

Each of the closed-system models significantly overestimates the temperature of the ankerite-out reaction (Fig. 3). At a pressure of 8 kbars, models for 189a and Wep-29a never achieve this reaction; i.e., it is predicted to occur at >650 °C, outside the model domain. The closed-system model for 184a predicts ankerite-out at 620 °C. On the other hand, the fluid-infiltrated models with $X_{CO_2} = 0.05$ predict ankerite breakdown at either 500 or 505 °C, which is well within the expected temperature range.

Fig. 4 shows the temperatures of major isograd reactions as predicted by fluid-infiltrated models at a range of X_{CO_2} values. The independently constrained reaction temperatures are shown as shaded bars for comparison. In general, an increase in the X_{CO_2} of the fluid corresponds to an increase in the temperature of each reaction. When $X_{CO_2} = 0.025$ each reaction is predicted to occur at a low temperature that is inconsistent with independent constraints from Hewitt (1973) and Ague (2002). Conversely, when X_{CO_2} is on the higher end at 0.10 reactions are pushed to higher temperatures. Based on these reactions, we conclude that the "average" fluid composition lay mostly between $X_{CO_2} = 0.05$ and 0.10 during prograde metamorphism.

5.3. Mineral compositions

We calculate the Mg# (molar Mg/[Mg+Fe]) of several minerals which these models predict at a pressure of 8 kbars and a temperature marking the middle of the mineral's stability field. Predicted values in representative sample 184a are as follows: ankerite = 0.75, biotite = 0.72, amphibole = 0.86, and diopside = 0.69. We can compare these to actual measurements of mean Mg# (Ague, 2002) for ankerite, biotite, amphibole, and diopside; these are 0.76 ± 0.09, 0.65 ± 0.13, 0.71 ± 0.15, 0.70 ± 0.07 respectively ($\pm 2\sigma$ standard deviations of the measured population). In all cases, the model Mg# values are within the observed ranges.

5.4. Fluid compositions

Fig. 5 shows a calculated temperature-activity diagram and fluid evolution paths for representative sample 184a in closed or Rayleigh-like systems. Fluid is not present at low temperatures and first appears at 570 °C with a CO_2 activity (a_{CO_2}) of 0.48. As the temperature increases the a_{CO_2} for fully-closed and Rayleigh-like systems increases to a maximum of $a_{CO_2} = 0.83$ and $a_{CO_2} = 0.86$, respectively. This corresponds to X_{CO_2} values from 0.35 to 0.82 which, with one exception (W5), are significantly higher than the X_{CO_2} values reported by Ague (2002).

A temperature versus a_{CO_2} diagram for sample W5 is shown in Fig. 6. This sample has a markedly larger X_{CO_2} (0.55) than any others studied by Ague (2002). None of the calculated pseudosections predicted the observed mineralogy of W5, so they are not reproduced herein. There are, however, two small fields on the T–a_{CO_2} diagram which match the observed mineralogy (Fig. 6). At the peak temperature recorded by sample W5 (~615 °C from Ague, 2002) the lower highlighted phase field corresponds to an a_{CO_2} value of 0.46, and $X_{CO_2} = 0.33$. Fluid activity paths for fully-closed and Rayleigh-like evolution are also shown; these paths never intersect the regions representing the observed mineralogy, nor do they come particularly close.

5.5. Degree of decarbonation

Fig. 7 shows calculated decarbonation curves for all eight low-grade samples. The shaded bars indicate the prograde mass % CO_2 loss (kg CO_2 loss/total kg $CO_2 \times 100$) calculated by Ague (2003). He uses a completely independent approach, calculating mass-balance relative to an immobile reference species, Zr, established using a comprehensive evaluation of the geochemical reference frame.

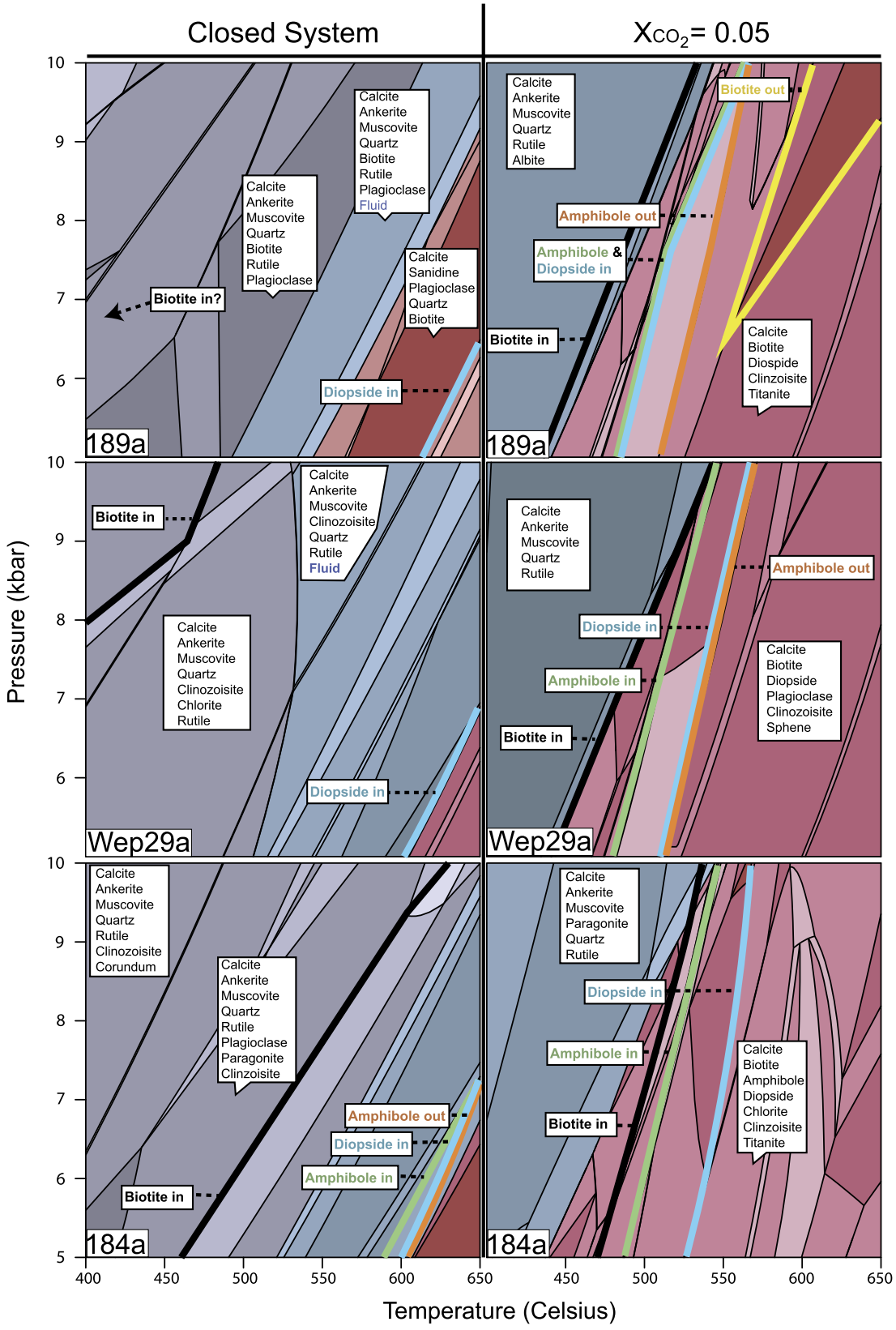

Fig. 3. Selected pseudosection results. The left column shows diagrams calculated in a fully closed-system; the right column shows diagrams calculated with fluid of $X_{CO_2} = 0.05$. Gray shaded regions indicate a phase field containing calcite and ankerite whereas red phase fields include only calcite. Sample names are shown on each panel.

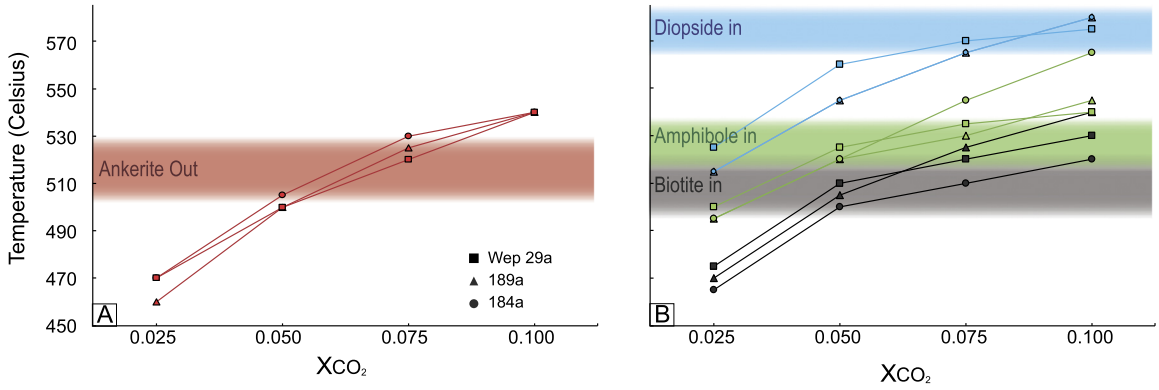

Fig. 4. Temperatures of major isograd reactions as predicted by fluid-infiltrated models at a range of X_{CO_2} values. Different symbols correspond to different samples. Black curves are for the biotite-in reaction, green curves for amphibole-in, and blue curves for diopside-in. The ankerite-out reaction is shown in red in part A). The independently constrained reaction temperatures from Ague (2002) are shown as shaded bars for comparison. In all cases an increase in X_{CO_2} corresponds to reaction at higher temperatures.

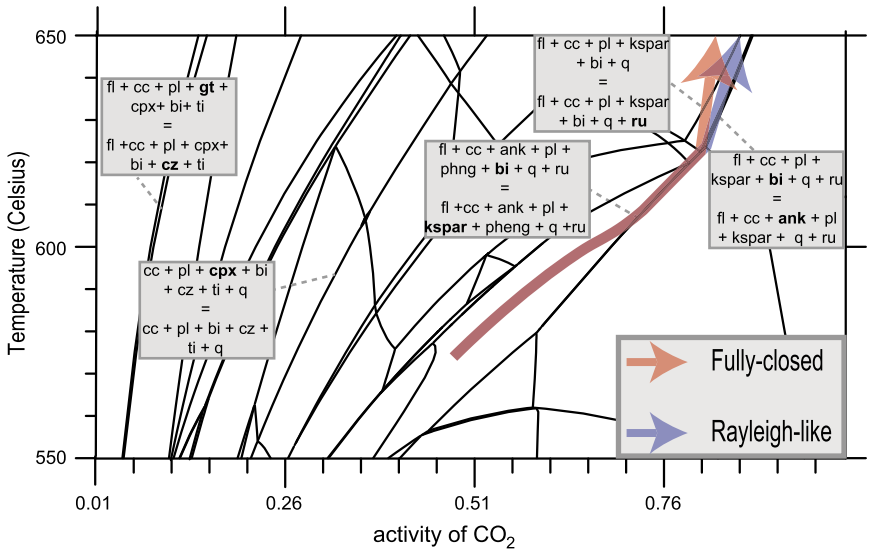

Fig. 5. Temperature versus activity of CO_2 diagram for representative sample 184a at $P = 8$ kbars. Solid black lines indicate univariant reaction curves. The red and blue arrows indicate the calculated fluid path of a fully-closed or Rayleigh-like system respectively. Several key reactions are shown in gray boxes with the product side always indicating the higher a_{CO_2} assemblage. Bold face denotes phases present on only one side of a reaction. Abbreviations: cc, calcite; pl, plagioclase; gt, garnet; cpx, clinopyroxene, bi, biotite; ti, titanite; cz, clinozoisite; q, quartz; phng, phengite; ru, rutile; ank, ankerite; kspar, K-feldspar.

Fully-closed and Rayleigh-like models significantly underestimate the % mass CO_2 loss, with values peaking around ~10 to 15%. Conversely, the fluid-infiltrated models are in excellent agreement with the independent constraints and predict peak decarbonation corresponding to ~50% CO_2 loss.

6. Discussion

6.1. Fluid infiltration

The closed-system approach consistently makes inaccurate predictions. *No* fully-closed pseudosection correctly reproduces the mineral zones observed in the field (Fig. 3). Each fully-closed model overestimates the temperature of ankerite breakdown by at least 100 °C. Furthermore, the metamorphic fluids created in these closed-system models are very CO_2-rich (Fig. 5), which is at odds with independent constraints on fluid compositions in the Wepawaug Schist (Ague, 2002). We therefore conclude that the modern rock composition is *not* representative of the reactive system at the time of metamorphism and that a water-bearing fluid must have infiltrated the metacarbonate units.

The source of this fluid may be largely quite local (i.e. outcrop-scale); the intercalated metaclastic rocks – by far the bulk of the volume of the Wepawaug Schist – released considerable H_2O during prograde metamorphism (Ague, 2000; Ague and Rye, 1999). This metamorphic fluid could then infiltrate the smaller volume of metacarbonate layers and drive reaction. In systems with fewer water-rich rocks, fluid infiltration may be more limited (e.g. Gorman et al., 2006).

In the Wepawaug Schist, however, there is evidence for very large channelized time-integrated fluid fluxes on the order of $\sim 10^5\ m^3\ m^{-2}$ in the higher-grade zones (Ague, 2003). Furthermore, the isotope record in the diopside zone suggests infiltration of magmatically sourced fluids with $\delta^{18}O$ values much lower than the country rock (Palin, 1992; Tracy et al., 1983; see also Ferry, 1992; Léger and Ferry, 1993). Thus, the fluids which entered the metacarbonate rocks may have been derived from a combination of outcrop-scale clastic dewatering and further-field dehydration and degassing of magmatic intrusions (Palin, 1992; van Haren et al., 1996; Lancaster et al., 2008). Regardless of the source, an externally-derived fluid is essential in explaining the observed prograde mineral succession and fluid compositions.

Our results also indicate that most fluid had a low X_{CO_2}. Pseudosections calculated with $X_{CO_2} = 0.05$ are in agreement with independent constraints on the evolution of these rocks. Lowering the X_{CO_2} to 0.025 pushes all of the reactions to lower tempera-

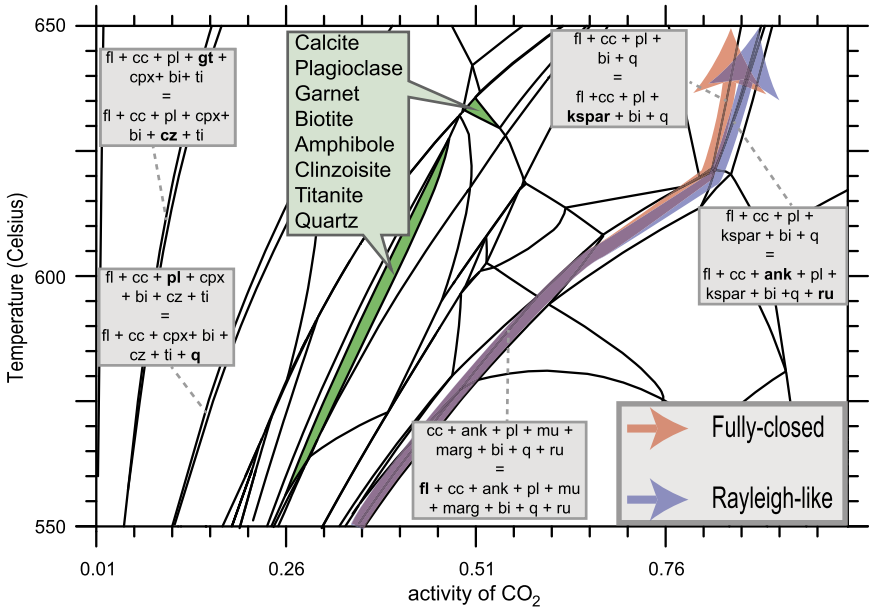

Fig. 6. Temperature versus activity of CO_2 diagram for sample W5 at $P = 8$ kbars. Shaded green fields match the observed mineralogy of W5. The red and blue arrows indicate the calculated fluid path of a fully-closed or Rayleigh-like system respectively. These fluid paths never intersect the highlighted phase fields. Several key reactions are shown in gray boxes with the product side always indicating the higher a_{CO_2} assemblage. Abbreviations as in Fig. 5. Additionally: fl, fluid; mu, muscovite; marg, margarite.

tures (e.g. ankerite-out occurs at 8 kbars and 460 °C) that are not consistent with independent constraints. On the other hand, raising the X_{CO_2} to 0.075 increases the temperature of each reaction. The phase diagrams calculated at $X_{CO_2} = 0.075$ are still consistent with the result of Ague (2002). Those calculated with $X_{CO_2} = 0.10$ are not consistent with lower-grade isograd reactions (i.e. ankerite-out and biotite-in) but *are* consistent with the diopside-in reaction at higher-grade (Fig. 4). Based on this relationship, we suggest that the best estimate for the X_{CO_2} of the metamorphic fluid is between ~0.05 and ~0.075 during ankerite-out reaction, and that it may have increased to ~0.10 at higher-grade (Ferry, 2016 documents a similar relationship between X_{CO_2} and grade). These estimates fall well within the range of X_{CO_2} values that would be expected to equilibrate with graphitic metapelitic rocks (~0.02 to ~0.20 from Connolly and Cesare, 1993) and are, thus, consistent with the interpretation that an infiltrating fluid equilibrated with the intercalated graphite-bearing schists. Moreover, the estimates also agree with the average value from Ague (2002; $X_{CO_2} = 0.08$), although of course both somewhat higher and lower values are also recognized.

The infiltration history of sample W5 likely differs from the others. Fluid-infiltrated pseudosections at low X_{CO_2} values do not reproduce its observed mineralogy, and the matching phase-field on the T–a_{CO_2} diagram suggests a fluid composition of $X_{CO_2} = 0.33$ (see above discussion and Fig. 6). The fully-closed and Rayleigh-like fluid evolution curves for W5 do not successfully reproduce this value at the peak temperature of 615 °C. This demonstrates that some open-system infiltration must have affected W5; however, the X_{CO_2} of the fluid attained significantly higher values than throughout most of the Wepawaug Schist. Perhaps the infiltrating fluid had a locally higher X_{CO_2} to begin with. Alternatively, if W5 was infiltrated by only a small amount of water-bearing fluid and subsequently isolated from the flow system, the resulting decarbonation reactions may have been sufficient to raise the X_{CO_2} of the fluid to higher values (e.g. Ague and Rye, 1999; Ferry, 2016). In addition, the constant 8 kbar pressure assumption for modeling the history of this sample may be inadequate, given that it records a peak pressure of ~9.5 kbars. The precise history remains unknown, but regardless, W5 must have undergone some open-system processes to produce its observed mineralogy.

6.2. Metamorphic decarbonation

Perhaps the most significant result is the degree to which fluid-infiltration drives decarbonation. Fluid-infiltrated models predict much greater CO_2 loss than the closed-system or Rayleigh-like models (Fig. 7). At peak conditions, we calculate ~50% CO_2 loss via forward modeling of these fluid-infiltrated lithologies. Conversely, the closed-system and Rayleigh-like models predict only ~10 to ~15% CO_2 loss at peak conditions, underestimating the degree of local decarbonation by a factor of five. The models are even more divergent at lower temperatures (below 600 °C) where fluid-infiltrated models predict up to ~45% CO_2 loss and, remarkably, closed-system models predict <1% decarbonation.

The degree of divergence between closed-system models and fluid-infiltrated models is temperature dependent. At very low temperatures (i.e. <~500 °C) both fluid-infiltrated and closed-system models predict minimal (<~5%) decarbonation. At moderate temperatures between ~500 and 650 °C the models diverge (Fig. 7). However, at higher temperatures they converge somewhat. For example, by 800 °C in the granulite facies sample 184a is predicted to achieve 41% CO_2 loss in a fully closed-system versus 50% CO_2 loss with a fluid composition of $X_{CO_2} = 0.05$. The closed-system model still estimates a lower degree of decarbonation, but the difference is smaller than predicted for the greenschist and amphibolite facies.

We emphasize that the phenomenon of fluid-driven decarbonation is not peculiar to this area. It has been documented in a number of regional settings and tectonic environments (e.g. Bebout and Carlson, 1986; Cook-Kollars et al., 2014; Ferry, 1983, 1992, 2016; Kleine et al., 2016; Léger and Ferry, 1993; Williams et al., 1996). It may, in fact, be more ubiquitous than has already been recognized. In more sparsely-studied or poorly-exposed regions with weaker pressure–temperature constraints, one could miss the evidence for fluid-infiltration.

6.3. Estimating a metamorphic CO_2 flux

6.3.1. Constructing a numerical model

With these results, we can estimate a regional flux of CO_2 from the Wepawaug Schist as a result of metamorphism. A simple

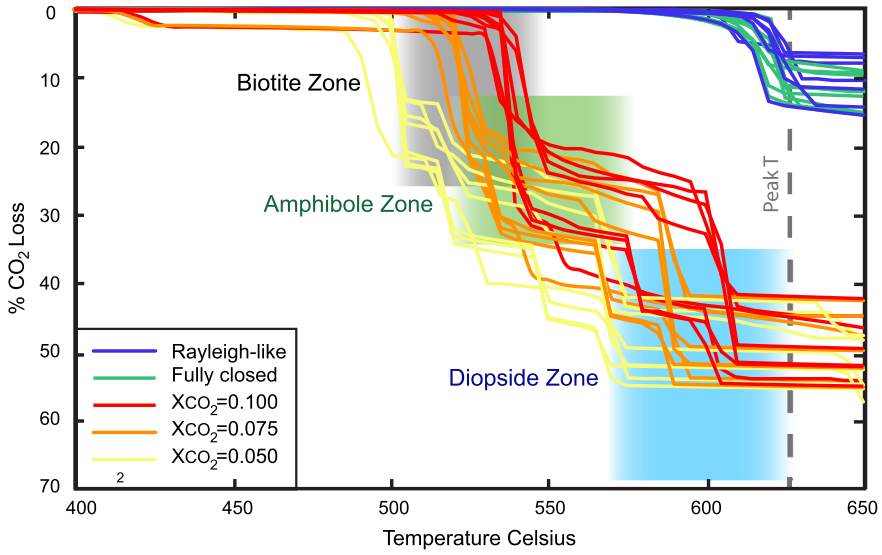

Fig. 7. Temperature vs. CO_2 loss for the eight ankerite zone precursors. The type of calculation is keyed to the color of each calculated curve. For example, each of the eight red curves was calculated using a fluid-infiltrated model at $X_{CO_2} = 0.10$. Shaded boxes correspond to the temperature and carbon loss conditions experienced in each of the major mineral zones as determined by Ague (2003).

model is constructed using heating rates and absolute age constraints from Lancaster et al. (2008), the field temperature gradient from Ague (2002), and the temperature versus CO_2-loss relationship from this study (Fig. 7) to calculate the fraction of CO_2 lost across a profile of the Wepawaug Schist over time (Appendix B). These fractional loss values are integrated across the spatial profile and then converted to total CO_2 released according to the following equation:

$$F = f_{lost} \cdot f_{vol} \cdot f_{CO_2} \cdot z \cdot \rho \cdot M_{CO_2}^{-1} \quad (1)$$

where F is the total areal flux, f_{lost} is the fraction of CO_2 devolatilized, f_{vol} is the volume fraction of metacarbonate rocks in the unit, f_{CO_2} is the initial weight fraction of CO_2 in the rock, z is the thickness of the unit, ρ is the rock density of the entire sequence, and M_{CO_2} is the molar mass of CO_2. Uncertainty propagation is described in Appendix B.

The resulting time versus degassed CO_2 curve (Fig. 8) predicts that metacarbonate rocks degas between 0.49×10^{13} and 1.8×10^{13} mol CO_2 km^{-2} over a period of ~15 Myr. This result incorporates both the spatial heterogeneity in peak temperature and the non-linear relationship between temperature and decarbonation.

We must also consider extreme decarbonation in calc-silicate layers that form at the contacts between metacarbonate and metapelitic rocks and in reaction selvages adjacent to quartz veins (Ague, 2003; Tracy et al., 1983). Although they make up a small proportion (~1%) of the unit volume, they underwent a high degree of devolatilization (~90% CO_2 loss; Ague, 2003) and are therefore significant to the net CO_2 flux. We perform a simpler calculation for calc-silicates in which only the final amount of CO_2 degassed is determined via an analogous simulation (Appendix B). This yields a total calc-silicate decarbonation flux of 0.25×10^{13} to 0.71×10^{13} mol CO_2 km^{-2} (Fig. 8). We can quite reasonably assume that the calc-silicate layers underwent their decarbonation during the same ~15 Myr when the intercalated metacarbonate rocks were devolatilizing (Fig. 8).

Note that we do not include decarbonation from higher-grade rocks (sillimanite zone) in neighboring rock units to the west of the field area because their degree of decarbonation is poorly constrained as is the critical degree of fluid infiltration. Although they make up a relatively small volume of the metamorphic belt, including an analysis of these units would increase any CO_2 flux estimate somewhat.

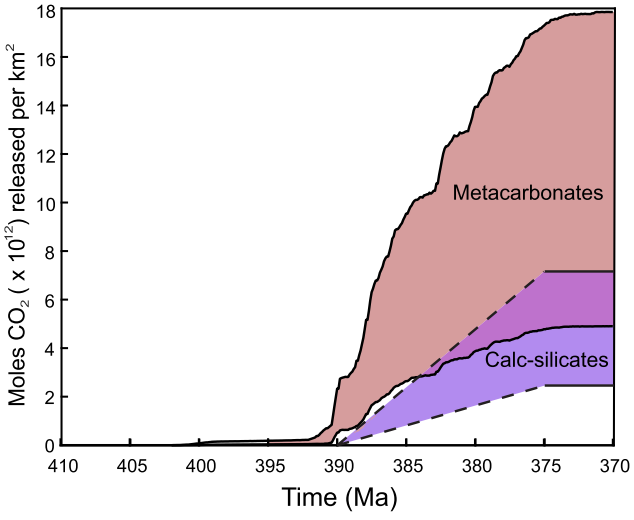

Fig. 8. Time versus areal CO_2 degassing curves. The red curve is the calculated decarbonation in metacarbonate units. The range of values shown indicates the 5th and 95th percentiles resulting from the simulation. The purple curve shows the result of a simpler calculation for calc-silicate layers in which only the final value is determined and the emitted CO_2 is assumed to increase linearly over 15 Myr. The range of values corresponds to the 5th and 95th percentile results. The total decarbonation of the Wepawaug Schist would be the sum of the red and purple curves.

In summary, we estimate that the Wepawaug Schist contributed between 0.74×10^{13} and 2.5×10^{13} mol CO_2 km^{-2}. As the vast majority of decarbonation occurred over ~15 Myr (Fig. 8), the resulting average rate is 0.50×10^{12} to 1.7×10^{12} mol CO_2 km^{-2} Myr^{-1}.

6.3.2. Magnitude of the orogenic CO_2 flux

Our flux estimate is strikingly similar to existing estimates of orogenic CO_2 release made using a variety of independent methods (Fig. 9). For example, Becker et al. (2008) estimate a modern flux of 1.2×10^{12} mol CO_2 km^{-2} Myr^{-1} in hydrothermal springs of the Himalaya (converted from units of 0.9×10^{12} mol CO_2 yr^{-1} over an area of 7.5×10^5 km^2). Our calculated rate of 0.50×10^{12} to 1.7×10^{12} mol CO_2 km^{-2} Myr^{-1} overlaps with this estimate.

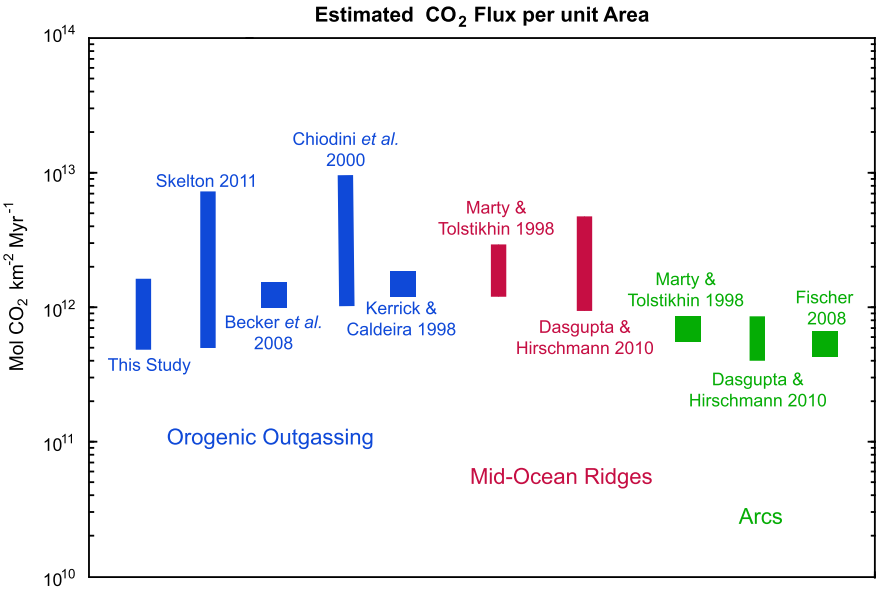

Fig. 9. Area-normalized CO_2 flux estimates from this study and others (see Appendix C). Squares indicate single reported values. Bars indicate a range of values, not necessarily a normal distribution. Flux estimates from Mid-Ocean Ridge and Arc volcanoes are also shown for reference.

Chiodini et al. (2000) measure modern CO_2 degassing in cold springs of the eastern Apennines, Italy. Through a combination of mass-balance calculations and isotopic measurements, they conclude that a deep CO_2 source (including both metamorphic and igneous components) contributes a diffuse flux of $\sim 10^{12}$ to 9.3×10^{12} mol CO_2 km^{-2} Myr^{-1}; our estimates are comparable.

Skelton (2011) calculates a flux of 0.5×10^{12} to 7×10^{12} mol CO_2 km^{-2} Myr^{-1} for greenschist facies decarbonation in the Scottish Highlands (originally reported as 0.5–7 mol CO_2 m^{-2} yr^{-1}). A time-integrated fluid flux is calculated using a combination of (1) chromatographic modeling to determine a Peclet number, (2) direct measurements of tortuosity, (3) empirical diffusion rates for CO_2 and (4) a calculated time-averaged porosity. Mineral equilibria are then used to constrain the fluid composition, resulting in a total CO_2 flux rate. The timescale of flow in Skelton (2011) was highly transient (<10 kyr) but remarkably, despite a totally independent method of calculation, the flux estimate compares well with ours.

Kerrick and Caldeira (1998) estimate a flux of 1.5×10^{12} mol CO_2 km^{-2} Myr^{-1} in northern New England (taken as an analogue for the Cordilleran belt) using time-integrated fluid-fluxes and fluid compositions from Léger and Ferry (1993). This number is close to our estimate as well. While Kerrick and Caldeira (1998) suggest that the nearby magmatism is necessary for metamorphism in this setting, the critical driver of reaction progress is fluid-infiltration which need not necessarily be magmatically sourced.

Remarkably, each of the above flux estimates has a comparable magnitude. Whether via direct measurement of modern CO_2 outgassing or inferences made in ancient orogenic belts, researchers consistently estimate an orogenic flux of $\sim 10^{12}$ mol CO_2 km^{-2} Myr^{-1}. Fig. 9 depicts the confluence of all of these independent constraints (see Appendix C). Volcanogenic fluxes from mid-ocean ridges (Dasgupta and Hirschmann, 2010; Marty and Tolstikhin, 1998) and island arcs (Dasgupta and Hirschmann, 2010; Fischer, 2008; Marty and Tolstikhin, 1998) are also shown for reference (although note that these may have changed significantly throughout geologic time, e.g. Lee et al., 2013). The magnitude of the orogenic flux is comparable to volcanogenic outgassing when normalized to area. In fact, estimates even tend to exceed the flux from arc volcanoes.

These results have several important implications. First, they suggest that metamorphic degassing may be a significant source of CO_2 on a global scale. As Becker et al. (2008) note, these fluxes exceed estimates for weathering-driven CO_2 draw-down (e.g. Galy and France-Lanord, 1999). Thus metamorphism and orogenesis must be considered as possible drivers of warming in Earth's past (e.g. Bickle, 1996; Kerrick and Caldeira, 1998). Second, the good agreement between measured surface fluxes and estimates of deep CO_2 production indicates that there may be minimal reprecipitation or trapping of CO_2 after decarbonation reactions. For example, we calculate a maximum of 1.7×10^{12} mol CO_2 km^{-2} Myr^{-1} are produced at depth. To result in the surface flux of 1.2×10^{12} mol CO_2 km^{-2} Myr^{-1} measured by Becker et al. (2008), ~70% of the produced CO_2 must ultimately make it to the atmosphere; this ~30% mismatch may be attributable to retrograde carbonation (e.g. Kleine et al., 2015). Using the surface fluxes from Chiodini et al. (2000) indicates even more CO_2 escapes (although the highest fluxes in the Apennines could include some magmatic component).

Of course, the flux estimate calculated herein is only for the Wepawaug Schist. Nevertheless, the close convergence of multiple lines of evidence leads us to propose that a flux of $\sim 10^{12}$ mol CO_2 km^{-2} Myr^{-1} may represent metamorphism of lithologically heterogeneous metasedimentary sequences more generally.

6.3.3. *Acadian CO_2 flux*

With a few assumptions we can extrapolate our results to the area of the entire Acadian orogenic belt. First, we take the Wepawaug Schist as representative of the belt as a whole. Similar intercalated metasedimentary sequences are present throughout the Appalachians (e.g. Ferry, 1992 in Vermont; Wehr and Glover, 1985 in the Blue Ridge; Kindle and Whittington, 1958 in western Newfoundland). Where deeper crust is exposed, it is reasonable to conclude that these (meta)sedimentary sequences were present and have been eroded away. Note that our model assumes ~10% of the metasedimentary volume is composed of carbonate rocks; even using a high metasedimentary thickness of 20 km, this corresponds to 2 km of carbonate out of a typical 70 km orogenic crustal thickness, or ~3% of the orogenic volume. Most significantly, the close correspondence between our Wepawaug flux estimate and orogenic flux estimates from the literature bolsters the argument that

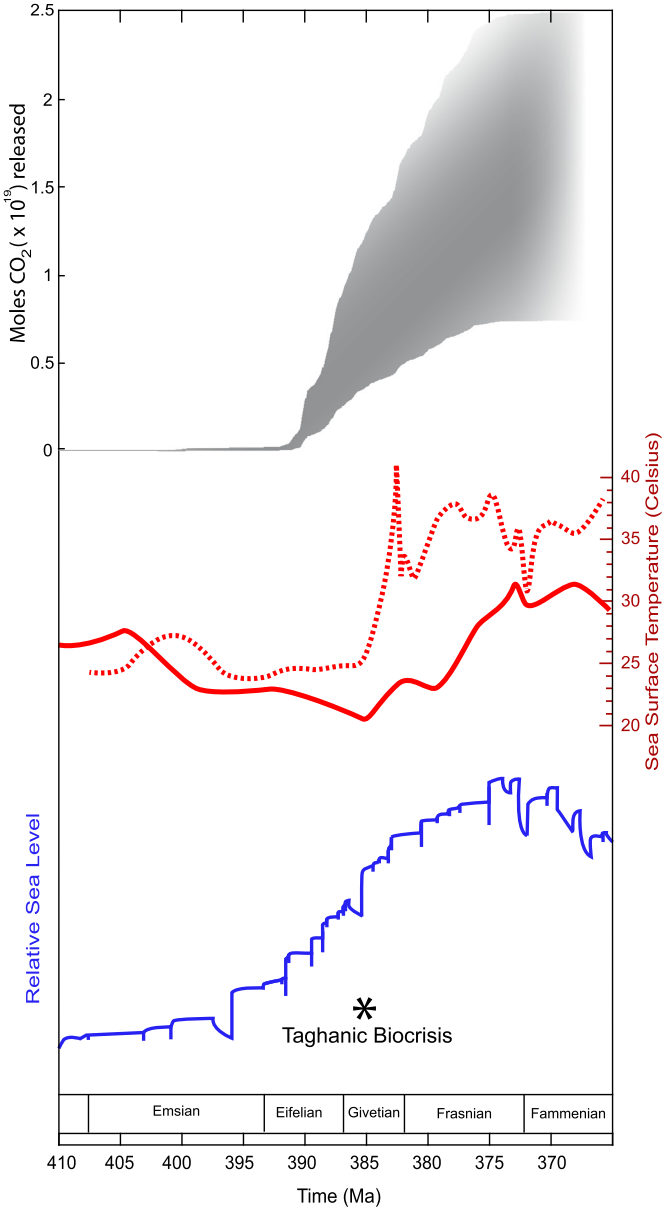

Fig. 10. Relative timing of Acadian degassing, global warming, and marine transgression (see Appendix D). The gray curve shows the calculated range of CO_2 degassing for the Acadian belt as a whole. The two red lines are sea surface temperature estimates derived from the oxygen isotope record. The dashed line is from van Geldern et al. (2006), the solid line from Joachimski et al. (2009). The blue curve shows relative sea level (Brett et al., 2011 after Johnson et al., 1985). The approximate timing of the Taghanic Biocrisis is also indicated.

Wepawaug decarbonation is representative of broad orogenic decarbonation. We therefore multiply our areal flux by the area of the Acadian metamorphic belt (taken as $\sim 10^6$ km^2 from the New York promontory in the South to Newfoundland in the North) to estimate the moles of CO_2 released across the entire orogen. The resultant total is $\sim 0.74 \times 10^{19}$ to 2.5×10^{19} mol CO_2 (Fig. 10).

Second, we assume that the timescales of metamorphism in the Wepawaug Schist are representative of the Acadian belt as a whole. Geochronologic work indicates Acadian metamorphism occurring from ~408 Ma (e.g. Zeitler et al., 1990) to ~380 Ma (e.g. Sullivan, 2014). While the docking of Avalonia and corresponding deformation may have begun significantly earlier (~420 Ma; van Staal et al., 2009), radiometric ages indicate that metamorphism did not begin until somewhat later (e.g. Lancaster et al., 2008 and Sullivan, 2014 in Connecticut; Valverde-Vaquero et al., 2000 in Newfoundland; Zeitler et al., 1990 in New Hampshire). Within a maximum bracketed metamorphic duration of ~25 Myr, our ~15 Myr interval for CO_2 release is a reasonable rough estimate for the entire mountain belt. Thus we calculate a total regional flux of 0.50×10^{18} to 1.7×10^{18} mol CO_2 Myr^{-1} (Fig. 10). If, instead, significant decarbonation in the region occurred over the maximum time interval we would see a reduction in the calculated *rate* of CO_2 release by as much as ~50%, but the total amount of CO_2 released is insensitive to this value.

It is possible that the degree of infiltration – and therefore decarbonation – experienced by the Wepawaug Schist is not representative of the broader Appalachians. However, work by Ferry (1976, 1992, 1994, and 2016) and Léger and Ferry (1993) in Maine and Vermont is consistent with our results. In fact, these studies usually indicate a somewhat higher degree of decarbonation affecting a larger volumetric proportion of carbonate rocks (Ague, 2014). Furthermore, decarbonation of metapelitic and metapsammitic lithologies has been documented elsewhere in New England (e.g. Ferry, 2007) which would further increase the flux, although we note that carbonate minerals are uncommon in the metaclastic rocks of the Wepawaug. Therefore, we are confident that using Wepawaug decarbonation as a model basis will not overestimate regional decarbonation over the entire metamorphic belt.

6.3.4. Devonian warming, sea level rise, and extinctions

Kerrick and Caldeira (1993) estimate that a flux of $\sim 10^{18}$ mol CO_2 Myr^{-1} would be required for metamorphic degassing to have a measurable effect on Earth's climate. Our maximum rate of 1.7×10^{18} mol CO_2 Myr^{-1} across the entire orogenic belt exceeds this number and, thus, we speculate that it may have been sufficient to perturb climate. The synchronous cooling resulting from enhanced silicate weathering and organic carbon burial associated with orogenesis would be expected to have a dampening effect. Nonetheless, our results suggest massive Acadian CO_2 input into the Devonian atmosphere.

Indeed, there is evidence of global warming, marine transgression, and extinction at precisely this time. The middle- to late-Devonian is characterized by global sea level rise (Brett et al., 2011; Johnson et al., 1985) including the dramatic transgression of the "Taghanic Onlap" (Johnson, 1970) during the middle Givetian (~385 Ma). The corresponding Taghanic Biocrisis is characterized by the synchronous extinction of cold-water taxa (e.g. De Melo, 1989) and latitudinal expansion of warm-water ammonoids and brachiopods (Boucot and Theron, 2001; House, 1978). Oxygen isotope records also indicate warming during this period (Joachimski et al., 2009; van Geldern et al., 2006). The cause of this warming has thus far remained enigmatic (Aboussalam and Becker, 2011).

The brief warming and marine transgression associated with the Taghanic Biocrisis are superimposed on a broader trend of increasing temperature and rising sea level from ~395 to ~375 Ma. This coincides with the timing of Acadian decarbonation via our analysis (Fig. 10). This close concurrence is, at least to first order, suggestive of some relationship (Appendix D).

The Taghanic Biocrisis and associated transgression are themselves fairly abrupt, occurring over <1 Myr (Aboussalam and Becker, 2011). Our modeled decarbonation cannot readily account for such a short-lived period of warming. However, the relatively recent recognition of metamorphic "pulses" in the type-locality for Barrovian metamorphism (e.g. Ague and Baxter, 2007; Viete et al., 2011) suggests that similar short-lived metamorphic processes may remain unrecognized in other orogenic belts. Indeed, Skelton (2011) documents Barrovian decarbonation on a very short timescale (<10 kyr). We therefore speculate that a comparable Acadian metamorphic pulse superimposed on longer progressive devolatilization could have conceivably resulted in transient decarbonation and climatic effects.

In present-day Europe, the related Scandian phase of the Caledonian Orogeny is largely complete by this time with only low-grade retrograde metamorphism occurring at ~395 Ma (Essex and Gromet, 2000). Meanwhile the Variscan Orogeny is just beginning, with $^{40}Ar/^{39}Ar$ ages recording metamorphism as early as ~390 Ma in Spain (e.g. Dallmeyer et al., 1997). Either of these two events may have contributed additional metamorphic CO_2 to the atmosphere; however, as they are primarily asynchronous, we expect that their effects during this particular time interval will be overshadowed by Acadian decarbonation.

The much smaller Ellesmerian and Antler Orogenies also began in the Devonian (e.g. Colpron and Nelson, 2009). However, they occurred well after warming and transgressive trends had already begun and are therefore not plausibly connected to pre-Frasnian warming. Similarly, the eruption of the Viluy Traps began around ~377 Ma (Ricci et al., 2013) and cannot explain earlier warming trends. We therefore propose that the Acadian Orogeny is a potential tectonic driver of mid-Devonian climate change. Infiltration-driven decarbonation may have been a source of atmospheric CO_2 that contributed to global warming and the corresponding eustatic fluctuation and extinction in the mid- to late-Devonian.

7. Conclusions

Fluid infiltration is essential to explain the prograde mineral succession, degree of decarbonation, and fluid compositions observed in the metacarbonate rocks of the Wepawaug Schist, CT. Purely closed-system models of metamorphism produce untenable results with respect to practically any qualitative or quantitative observable. On the other hand, approximating fluid infiltration by performing pseudosection analysis with a set of fixed X_{CO_2} values works remarkably well to reproduce the prograde reaction and CO_2 loss which these rocks underwent in nature.

Our results highlight the fact that the carbonate-producing reactions cannot be modeled without knowledge of the amount and nature of aqueous fluid infiltration, reinforcing earlier open-system interpretations of metacarbonate rock petrogenesis in New England (e.g. Ague, 1994, 2000, 2003; Ague and Rye, 1999; Ferry, 1983, 1992, 2016; Palin, 1992; Tracy et al., 1983). Infiltrating H_2O-bearing fluid drove significant (~50%) progressive CO_2 loss from greenschist through amphibolite facies. Thus, given sufficient fluid-infiltration, very high temperatures (e.g. granulite facies) are not required to achieve major decarbonation.

The areal flux of 0.50×10^{12} to 1.7×10^{12} mol CO_2 km^{-2} Myr^{-1} we calculate for the Wepawaug Schist is consistent with multiple other metamorphic outgassing estimates from the literature; we suggest that ~10^{12} mol CO_2 km^{-2} Myr^{-1} may be representative of orogenic degassing in general. This is greater than or comparable to estimates for the areal volcanogenic flux of CO_2 from mid-ocean ridges and arcs.

Finally, we extrapolate this result to the entire Acadian Orogen for a total flux of 0.50×10^{18} to 1.7×10^{18} mol CO_2 Myr^{-1}. This could have been sufficient to drive global climate change (Kerrick and Caldeira, 1993). The synchronicity of Acadian degassing and the mid- to late-Devonian marine transgression and biocrisis indicates a possible causal link between regional metamorphism and climate-driven extinction.

Acknowledgements

We thank G.E. Bebout, R.A. Berner, O. Beyssac, A.V. Brovarone, C.P. Chamberlain, B. Marty, F. Piccoli, N.J. Planavsky, D. Rumble, D.M. Rye, and J.L.M. van Haren for stimulating and helpful discussions, and J.M. Ferry and A.D.L. Skelton for thorough and constructive reviews. The Reservoirs and Fluxes Community of the Deep Carbon Observatory is thanked for supporting a workshop on Tectonic Fluxes of Carbon. We gratefully acknowledge financial support from National Science Foundation grants EAR-9706638, EAR-9810089, and EAR-1650329.

Appendix. Supplementary material

Supplementary material related to this article can be found online at https://doi.org/10.1016/j.epsl.2018.02.028.

References

Aboussalam, Z.S., Becker, R.T., 2011. The global Taghanic Biocrisis (Givetian) in the eastern Anti-Atlas, Morocco. Palaeogeogr. Palaeoclimatol. Palaeoecol. 304 (1), 136–164.
Ague, J.J., 1994. Mass transfer during Barrovian metamorphism of pelites, south-central Connecticut; I, Evidence for changes in composition and volume. Am. J. Sci. 294 (8), 989–1057.
Ague, J.J., 2000. Release of CO_2 from carbonate rocks during regional metamorphism of lithologically heterogeneous crust. Geology 28 (12), 1123–1126.
Ague, J.J., 2002. Gradients in fluid composition across metacarbonate layers of the Wepawaug Schist, Connecticut, USA. Contrib. Mineral. Petrol. 143 (1), 38–55.
Ague, J.J., 2003. Fluid infiltration and transport of major, minor, and trace elements during regional metamorphism of carbonate rocks, Wepawaug Schist, Connecticut, USA. Am. J. Sci. 303 (9), 753–816.
Ague, J.J., 2014. Fluid flow in the deep crust. In: Holland, H.D., Turekian, K.K. (Eds.), Treatise on Geochemistry, vol. 4, 2nd edition. Elsevier, Oxford, pp. 203–247.
Ague, J.J., Baxter, E.F., 2007. Brief thermal pulses during mountain building recorded by Sr diffusion in apatite and multicomponent diffusion in garnet. Earth Planet. Sci. Lett. 261 (3), 500–516.
Ague, J.J., Rye, D.M., 1999. Simple models of CO_2 release from metacarbonates with implications for interpretation of directions and magnitudes of fluid flow in the deep crust. J. Petrol. 40 (9), 1443–1462.
Arrhenius, S., Sandström, J.W., 1903. Lehrbuch der kosmischen Physik 2.
Bebout, G.E, Carlson, W.D., 1986. Fluid evolution and transport during metamorphism: evidence from the Llano Uplift, Texas. Contrib. Mineral. Petrol. 92 (4), 518–529.
Becker, J.A., Bickle, M.J., Galy, A., Holland, T.J., 2008. Himalayan metamorphic CO_2 fluxes: quantitative constraints from hydrothermal springs. Earth Planet. Sci. Lett. 265 (3), 616–629.
Berman, R.G., 1991. Thermobarometry using multi-equilibrium calculations; a new technique, with petrological applications. Can. Mineral. 29 (4), 833–855.
Berner, R.A., 1989. Biogeochemical cycles of carbon and sulfur and their effect on atmospheric oxygen over Phanerozoic time. Global Planet. Change 1 (1–2), 97–122.
Bickle, M.J., 1996. Metamorphic decarbonation, silicate weathering and the long-term carbon cycle. Terra Nova 8 (3), 270–276.
Boucot, A.J., Theron, J.N., 2001. First Rhipidothyris (Brachiopoda) from southern Africa: biostratigraphic, paleoecological, biogeographical significance. J. Geosci. 46 (3–4), 155–160.
Brett, C.E., Baird, G.C., Bartholomew, A.J., DeSantis, M.K., Ver Straeten, C.A., 2011. Sequence stratigraphy and a revised sea-level curve for the Middle Devonian of eastern North America. Palaeogeogr. Palaeoclimatol. Palaeoecol. 304 (1), 21–53.
Chamberlin, T.C., 1899. An attempt to frame a working hypothesis of the cause of glacial periods on an atmospheric basis. J. Geol. 7 (6), 545–584.
Chiodini, G., Frondini, F., Cardellini, C., Parello, F., Peruzzi, L., 2000. Rate of diffuse carbon dioxide Earth degassing estimated from carbon balance of regional aquifers: the case of central Apennine, Italy. J. Geophys. Res., Solid Earth 105 (B4), 8423–8434.
Chu, X., Ague, J.J., 2013. Phase equilibria for graphitic metapelite including solution of CO_2 in melt and cordierite: implications for dehydration, partial melting and graphite precipitation. J. Metamorph. Geol. 31 (8), 843–862.
Colpron, M., Nelson, J.L., 2009. A Palaeozoic Northwest Passage: incursion of Caledonian, Baltican and Siberian terranes into eastern Panthalassa, and the early evolution of the North American Cordillera. Geol. Soc. (Lond.) Spec. Publ. 318 (1), 273–307.
Connolly, J.A.D., Cesare, B., 1993. C–O–H–S fluid composition and oxygen fugacity in graphitic metapelites. J. Metamorph. Geol. 11 (3), 379–388.
Connolly, J.A.D., Petrini, K., 2002. An automated strategy for calculation of phase diagram sections and retrieval of rock properties as a function of physical conditions. J. Metamorph. Geol. 20 (7), 697–708.
Cook-Kollars, J., Bebout, G.E., Collins, N.C., Angiboust, S., Agard, P., 2014. Subduction zone metamorphic pathway for deep carbon cycling: I. Evidence from HP/UHP metasedimentary rocks, Italian Alps. Chem. Geol. 386, 31–48.
Dallmeyer, R.D., Catalán, J.M., Arenas, R., Ibarguchi, J.G., Gutiérrez, G., Farias, P., Aller, J., 1997. Diachronous Variscan tectonothermal activity in the NW Iberian Massif: evidence from $^{40}Ar/^{39}Ar$ dating of regional fabrics. Tectonophysics 277 (4), 307–337.
Dasgupta, R., 2013. Ingassing, storage, and outgassing of terrestrial carbon through geologic time. Rev. Mineral. Geochem. 75 (1), 183–229.

Dasgupta, R., Hirschmann, M.M., 2010. The deep carbon cycle and melting in Earth's interior. Earth Planet. Sci. Lett. 298 (1), 1–13.

De Capitani, C., Petrakakis, K., 2010. The computation of equilibrium assemblage diagrams with Theriak/Domino software. Am. Mineral. 95 (7), 1006–1016.

De Melo, J.H.G., 1989. The Malvinokaffric Realm in the Devonian of Brazil. In: Mem. - Can. Soc. Pet. Geol., vol. 14, pp. 669–703.

Evans, K.A., Powell, R., Holland, T.J.B., 2010. Internally consistent data for sulphur-bearing phases and application to the construction of pseudosections for mafic greenschist facies rocks in Na_2O–CaO–K_2O–FeO–MgO–Al_2O_3–SiO_2–CO_2–O–S–H_2O. J. Metamorph. Geol. 28 (6), 667–687.

Essex, R.M., Gromet, L.P., 2000. U–Pb dating of prograde and retrograde titanite growth during the Scandian orogeny. Geology 28 (5), 419–422.

Ferry, J.M., 1976. P, T, f_{CO_2}, and f_{H_2O} during metamorphism of calcareous sediments from the Waterville-Vassalboro area, south-central Maine. Contrib. Mineral. Petrol. 57, 119–143.

Ferry, J.M., 1983. Regional metamorphism of the Vassalboro Formation, south-central Maine, USA: a case study of the role of fluid in metamorphic petrogenesis. J. Geol. Soc. 140 (4), 551–576.

Ferry, J.M., 1992. Regional Metamorphism of the Waits River Formation, eastern Vermont, Delineation of a new type of giant metamorphic hydrothermal system. J. Petrol. 33, 45–94.

Ferry, J.M., 1994. Overview of the petrologic record of fluid flow during regional metamorphism in northern New England. Am. J. Sci. 294, 905–988.

Ferry, J.M., 2007. The role of volatile transport by diffusion and dispersion in driving biotite-forming reactions during regional metamorphism of the Gile Mountain Formation, Vermont. Am. Mineral. 92 (8–9), 1288–1302.

Ferry, J.M., 2016. Fluids in the crust during regional metamorphism: forty years in the Waterville limestone. Am. Mineral. 101 (3), 500–517.

Ferry, J.M., Winslow, N.W., Penniston-Dorland, S.C., 2013. Re-evaluation of infiltration-driven regional metamorphism in northern New England: new transport models with solid solution and cross-layer equilibration of fluid composition. J. Petrol. 54 (12), 2455–2485.

Fischer, T.P., 2008. Fluxes of volatiles (H_2O, CO_2, N_2, Cl, F) from arc volcanoes. Geochem. J. 42 (1), 21–38.

Franzolin, E., Schmidt, M.W., Poli, S., 2011. Ternary Ca–Fe–Mg carbonates: subsolidus phase relations at 3.5 GPa and a thermodynamic solid solution model including order/disorder. Contrib. Mineral. Petrol. 161 (2), 213–227.

Fritts C.E. (1963) Bedrock geology of the Mount Carmel quadrangle, Connecticut. U.S. Geological Survey Quadrangle Map GQ-199.

Fritts, C.E., (1965a). Bedrock geologic map of the Ansonia quadrangle, Fairfield and New Haven Counties, Connecticut. U.S. Geological Survey Quadrangle Map GQ-426.

Fritts, C.E., (1965b). Bedrock geologic map of the Milford quadrangle, Fairfield and New Haven Counties, Connecticut. U.S. Geological Survey Quadrangle Map GQ-427.

Galy, A., France-Lanord, C., 1999. Weathering processes in the Ganges–Brahmaputra basin and the riverine alkalinity budget. Chem. Geol. 159 (1), 31–60.

Gorman, P.J., Kerrick, D.M., Connolly, J.A.D., 2006. Modeling open system metamorphic decarbonation of subducting slabs. Geochem. Geophys. Geosyst. 7 (4).

Greenwood, H.J., 1975. Buffering of pore fluids by metamorphic reactions. Am. J. Sci. 275 (5), 573–593.

Groppo, C., Rolfo, F., Castelli, D., Connolly, J.A., 2013. Metamorphic CO_2 production from calc-silicate rocks via garnet-forming reactions in the CFAS–H_2O–CO_2 system. Contrib. Mineral. Petrol. 166 (6), 1655–1675.

Groppo, C., Rolfo, F., Castelli, D., Mosca, P., 2017. Metamorphic CO_2 production in collisional orogens: petrological constraints from phase diagram modeling of himalayan, scapolite-bearing, calc-silicate rocks in the NKC (F) MAS (T)-HC system. J. Petrol. 58 (1), 53–83.

Hayes, J.M., Waldbauer, J.R., 2006. The carbon cycle and associated redox processes through time. Philos. Trans. R. Soc. Lond. B, Biol. Sci. 361 (1470), 931–950.

Hewitt, D.A., 1973. The metamorphism of micaceous limestones from south-central Connecticut. Am. J. Sci. 273, 444–469.

Holland, T.J.B., Powell, R., 1998. An internally consistent thermodynamic data set for phases of petrological interest. J. Metamorph. Geol. 16 (3), 303–349.

House, M.R., 1978. Devonian Ammonoids from the Appalachians and Their Bearing on International Zonation and Correlation (No. 21). Palaeontological Association.

Jagoutz, O., Macdonald, F.A., Royden, L., 2016. Low-latitude arc–continent collision as a driver for global cooling. Proc. Natl. Acad. Sci. 113 (18), 4935–4940.

Joachimski, M.M., Breisig, S., Buggisch, W., Talent, J.A., Mawson, R., Gereke, M., Weddige, K., 2009. Devonian climate and reef evolution: insights from oxygen isotopes in apatite. Earth Planet. Sci. Lett. 284 (3), 599–609.

Johnson, J.G., 1970. Taghanic onlap and the end of North American Devonian provinciality. Geol. Soc. Am. Bull. 81 (7), 2077–2106.

Johnson, J.G., Klapper, G., Sandberg, C.A., 1985. Devonian eustatic fluctuations in Euramerica. Geol. Soc. Am. Bull. 96 (5), 567–587.

Kelemen, P.B., Manning, C.E., 2015. Reevaluating carbon fluxes in subduction zones, what goes down, mostly comes up. Proc. Natl. Acad. Sci. 112 (30), E3997–E4006.

Kerrick, D.M., 1977. The genesis of zoned skarns in the Sierra Nevada, California. J. Petrol. 18 (1), 144–181.

Kerrick, D.M., Caldeira, K., 1993. Paleoatmospheric consequences of CO_2 released during early Cenozoic regional metamorphism in the Tethyan orogen. Chem. Geol. 108 (1–4), 201–230.

Kerrick, D.M., Caldeira, K., 1998. Metamorphic CO_2 degassing from orogenic belts. Chem. Geol. 145 (3), 213–232.

Kerrick, D.M., Connolly, J.A.D., 2001a. Metamorphic devolatilization of subducted oceanic metabasalts: implications for seismicity, arc magmatism and volatile recycling. Earth Planet. Sci. Lett. 189 (1), 19–29.

Kerrick, D.M., Connolly, J.A.D., 2001b. Metamorphic devolatilization of subducted marine sediments and the transport of volatiles into the Earth's mantle. Nature 411 (6835), 293.

Kindle, C.H., Whittington, H.B., 1958. Stratigraphy of the Cow Head region, western Newfoundland. Geol. Soc. Am. Bull. 69 (3), 315–342.

Kleine, B.I., Pitcairn, I.K., Skelton, A.D., 2015. The mechanism of infiltration of metamorphic fluids recorded by hydration and carbonation of epidote–amphibolite facies metabasaltic sills in the SW Scottish Highlands. Am. Mineral. 100 (11–12), 2702–2717.

Kleine, B.I., Pitcairn, I.K., Skelton, A.D., 2016. Mineralogical controls on metamorphic fluid flow in metabasaltic sills from Islay, Scotland. Lithos 248, 22–39.

Kump, L.R., Brantley, S.L., Arthur, M.A., 2000. Chemical weathering, atmospheric CO_2, and climate. Annu. Rev. Earth Planet. Sci. 28 (1), 611–667.

Lancaster, P.J., Baxter, E.F., Ague, J.J., Breeding, C.M., Owens, T.L., 2008. Synchronous peak Barrovian metamorphism driven by syn-orogenic magmatism and fluid flow in southern Connecticut, USA. J. Metamorph. Geol. 26 (5), 527–538.

Lanzirotti, A., Hanson, G.N., 1996. Geochronology and geochemistry of multiple generations of monazite from the Wepawaug Schist, Connecticut, USA: implications for monazite stability in metamorphic rocks. Contrib. Mineral. Petrol. 125 (4), 332–340.

Lee, C.T.A., Shen, B., Slotnick, B.S., Liao, K., Dickens, G.R., Yokoyama, Y., Lenardic, A., Dasgupta, R., Jellinek, M., Lackey, J.S., Schneider, T., 2013. Continental arc–island arc fluctuations, growth of crustal carbonates, and long-term climate change. Geosphere 9 (1), 21–36.

Léger, A., Ferry, J.M., 1993. Fluid infiltration and regional metamorphism of the Waits River Formation, North-east Vermont, USA. J. Metamorph. Geol. 11 (1), 3–29.

Marty, B., Tolstikhin, I.N., 1998. CO_2 fluxes from mid-ocean ridges, arcs and plumes. Chem. Geol. 145 (3), 233–248.

Palin, J.M., 1992. Stable Isotope Studies of Regional Metamorphism in the Wepawaug Schist, Connecticut. Unpublished PhD thesis. Yale University, New Haven, CT.

Powell, R., Holland, T.J.B.H., Worley, B., 1998. Calculating phase diagrams involving solid solutions via non-linear equations, with examples using THERMOCALC. J. Metamorph. Geol. 16 (4), 577–588.

Ricci, J., Quidelleur, X., Pavlov, V., Orlov, S., Shatsillo, A., Courtillot, V., 2013. New $^{40}Ar/^{39}Ar$ and K–Ar ages of the Viluy traps (Eastern Siberia): further evidence for a relationship with the Frasnian–Famennian mass extinction. Palaeogeogr. Palaeoclimatol. Palaeoecol. 386, 531–540.

Sullivan, N.C., 2014. Advances in Samarium–Neodymium Geochronology: Applications to Early Earth Garnet, Hydrothermal Carbonate, and High Temperature Metamorphic Systems. Unpublished PhD thesis. Boston University, Boston, MA.

Skelton, A.D.L., 2011. Flux rates for water and carbon during greenschist facies metamorphism. Geology 39 (1), 43–46.

Tracy, R.J., Rye, D.M., Hewitt, D.A., Schiffries, C.M., 1983. Petrologic and stable-isotopic studies of fluid–rock interactions, south-central Connecticut: I. The role of infiltration in producing reaction assemblages in impure marbles. Am. J. Sci. 283, 589–616.

Valverde-Vaquero, P., Dunning, G.R., van Staal, C.R., 2000. The Margaree orthogneiss: an Ordovician, peri-Gondwanan, mafic-felsic igneous complex in southwestern Newfoundland. Can. J. Earth Sci. 37 (12), 1691–1710.

van Geldern, R., Joachimski, M.M., Day, J., Jansen, U., Alvarez, F., Yolkin, E.A., Ma, X.P., 2006. Carbon, oxygen and strontium isotope records of Devonian brachiopod shell calcite. Palaeogeogr. Palaeoclimatol. Palaeoecol. 240 (1), 47–67.

van Haren, J.L.M., Ague, J.J., Rye, D.M., 1996. Oxygen isotope record of fluid infiltration and mass transfer during regional metamorphism of pelitic schist, Connecticut, USA. Geochim. Cosmochim. Acta 60 (18), 3487–3504.

van Staal, C.R., Whalen, J.B., Valverde-Vaquero, P., Zagorevski, A., Rogers, N., 2009. Pre-Carboniferous, episodic accretion-related, orogenesis along the Laurentian margin of the northern Appalachians. Geol. Soc. (Lond.) Spec. Publ. 327 (1), 271–316.

Viete, D.R., Hermann, J., Lister, G.S., Stenhouse, I.R., 2011. The nature and origin of the Barrovian metamorphism, Scotland: diffusion length scales in garnet and inferred thermal time scales. J. Geol. Soc. 168 (1), 115–132.

Wehr, F., Glover III, L.Y.N.N., 1985. Stratigraphy and tectonics of the Virginia–North Carolina Blue Ridge: evolution of a late Proterozoic–early Paleozoic hinge zone. Geol. Soc. Am. Bull. 96 (3), 285–295.

Williams, I.S., Buick, I.S., Cartwright, I., 1996. An extended episode of early Mesoproterozoic metamorphic fluid flow in the Reynolds Range, central Australia. J. Metamorph. Geol. 14 (1), 29–47.

Zeitler, P.K., Barreiro, B., Chamberlain, C.P., Rumble, D., 1990. Ion-microprobe dating of zircon from quartz-graphite veins at the Bristol, New Hampshire, metamorphic hot spot. Geology 18 (7), 626–629.